https://doi.org/10.5194/essd-2026-782
Preprint. Discussion started: 22 November 2026
© Author(s) 2026. CC BY 4.0 License.



Open Access Earth System Science Data Discussions

Resolved gravity wave momentum flux dataset based on the ERA5 reanalysis

Zuzana Procházková[1] and Petr Šácha[1]

[1]Department of Atmospheric Physics, Faculty of Mathematics and Physics, Charles University, Prague, Czech Republic

Correspondence: Zuzana Procházková (prochazkova@karlin.mff.cuni.cz) and Petr Šácha (petr.sacha@matfyz.cuni.cz)

Abstract. Energy and momentum are redistributed in the atmosphere by gravity waves (GWs) mostly propagating upward from the troposphere. In current generation earth system models, GW effects need to be parameterized, which is one of the major causes of the uncertainty in projections of circulation changes. Here, we introduce a dataset of vertical fluxes of zonal and meridional momentum due to GWs resolved in ERA5 reanalysis, covering the vertical momentum transport by a part of the GW spectrum through a realistic stratospheric background (https://doi.org/10.5281/zenodo.22899283, Procházková and Šácha, 2026). The daily zonal mean data, divided into the contribution of waves with wavelengths from the effective resolution of ERA5 to wavelengths below 1000 and below 2000 km, cover the period 1979–2022 with high vertical and meridional resolution. We show that the distribution of the fluxes compares well with the satellite-based momentum estimates, although the magnitudes are underestimated. Finally, potential applications of the dataset in the research of climate effects of GWs are demonstrated on the examples of the quasi-biennial oscillation and sudden stratospheric warmings.

1 Introduction

Atmospheric gravity waves (GWs) are waves generated by the interplay of gravity and buoyancy force. They are continuously produced at various locations over the globe and propagate through the atmosphere. Since the waves transport momentum and energy, they can modify the background wind field. In the tropics, together with Kelvin waves and mixed Rossby-GWs, they contribute to the forcing of quasi-biennial oscillation (QBO)—an alternation of zonal and meridional winds with a period of approximately 28 months in the tropical stratosphere (Baldwin et al., 2001; Kim, 2025). The ability of models to represent the QBO is a lively topic of research, focusing on the depth of the oscillation and its amplitude (Richter et al., 2020). In the extratropics, among others, GWs also supplement planetary-wave forcing during sudden stratospheric warmings (SSWs), when the polar circulation changes abruptly and the temperature above the pole increases by tens of degrees (Baldwin et al., 2021; Limpasuvan et al., 2012; Ern et al., 2016), having an impact on the troposphere by shifting jet streams and causing extreme weather (Lim et al., 2019).

A key quantity describing the rate at which the momentum is transported upward by the wave and thus redistributed in the atmosphere is the momentum flux. In some form, momentum flux has previously been studied using satellite observations (Ern et al., 2004, 2016; Alexander et al., 2008), balloon observations (Hertzog et al., 2012; Green et al., 2024), or using high-resolution atmospheric models (Gupta et al., 2024a; Wei et al., 2022). Multiple datasets are available with estimates of

https://doi.org/10.5194/essd-2026-782
Preprint. Discussion started: 22 November 2026
© Author(s) 2026. CC BY 4.0 License.



Open Access Earth System Science Data Discussions

momentum fluxes from these studies. In particular, Gupta et al. (2024c) published 3 months of momentum flux estimates from 1km global model. From observational data, for example, the GRACILE dataset (Ern et al., 2018) provides the zonal means and global distributions of fluxes from satellite instruments High Resolution Dynamics Limb Sounder (HIRDLS) and Sounding of the Atmosphere using Broadband Emission Radiometry (SABER). All these datasets have, however, limited time span or vertical, horizontal or temporal resolutions, which prevents their broader utilization. In this work, we introduce daily estimates of zonal mean momentum flux due to GWs based on 44 years of ERA5 reanalysis, with an exceptionally high vertical and meridional resolution. The dataset presented here underlies the study (Procházková et al., 2025), which provided the first quasi-observational GW drag estimates. Moreover, by publishing the curated raw momentum fluxes here in the full vertical and meridional resolution, we aim to facilitate their broader utilization for specific research efforts in atmospheric dynamics, comparisons with observations and validation of GW parameterizations, where the momentum fluxes are the salient quantity.

In Sect. 2, the structure of the data is introduced, together with a brief description of the methodology applied to obtain the dataset. The data are compared to the satellite observation in Sect. 2.1. In Sect. 2.2, we show how the data can be used in connection with QBO or SSWs. Finally, the study is concluded by Sect. 4.

2 About the data

The presented dataset of GW momentum fluxes (Procházková and Šácha, 2026) was created based on the ERA5 reanalysis (Hersbach et al., 2020) and its extension for the years 2000 - 2006, ERA5.1 (Simmons et al., 2020). The dataset contains vertical levels between 120 and 5 hPa. Below 50 hPa, the ERA5 data on the model levels were interpolated to the pressure levels using linear interpolation. The levels above correspond directly to the model levels of the ERA5 reanalysis. The highest levels of the model are avoided due to a weak ERA5 sponge that dampens perturbations above the pressure level of 10 hPa and a stronger sponge, more important for GWs (Gisinger et al., 2022), acting above 1 hPa.

From the horizontal fields of the ERA5 data, GW perturbations were separated using the rhomboidal filter with two different settings, providing two estimates on the momentum fluxes. The first approach, here called the rho20 method, limits the zonal wavenumber m as $|m| \leq 20$ and the difference between the total wavenumber n and the size of the zonal wavenumber m as $n - |m| \leq 19$. The second one, called the rho40 method, uses the maximal zonal wavenumber 40 and the maximal difference between the total wavenumber and the size of the zonal wavenumber 39. The selection of the rhomboidal filter is motivated by the possibility to choose a partial zonal filtering within the GW separation procedure and avoids unphysically long wavelengths that are admitted by the traditional triangular truncation if the waves are not purely zonal or meridional. With these wavenumber limits, the wave perturbations considered in the estimates are allowed to have horizontal wavelengths up to approximately 2000 km for rho20 method and 1000 for rho40 method. Regarding the truncation methodology, we note that in our settings, the use of rhomboidal truncation generally results in negligible differences in the filtered fields from triangular truncation (Procházková et al., 2025).

The shortest horizontal wavelengths considered in the analysis are determined by the effective resolution of ERA5. Since the horizontal resolution of ERA5 is approximately 31 km and the effective resolution can be even 8 times higher (Klaver et al.,

https://doi.org/10.5194/essd-2026-782
Preprint. Discussion started: 22 November 2026
© Author(s) 2026. CC BY 4.0 License.



Open Access Earth System Science Data Discussions

2020; Abdalla, 2013), the data describe momentum fluxes produced by waves with the wavelengths 200–2000 km (rho20) and 200–1000 km (rho40). If not stated otherwise, the rho20 results will be shown in this paper. For the figures based on the rho40 method, please see the Supplement.

Using the selected perturbation part of the zonal and meridional velocity u' and v', the vertical flux of the zonal and meridional momentum (MF_{zx} and MF_{zy}) is computed using the formulas

$$MF_{zx} = \frac{1}{L}\int_L u'\omega' \mathrm{d}l, \tag{1}$$

$$MF_{zy} = \frac{1}{L}\int_L v'\omega' \mathrm{d}l, \tag{2}$$

where the integration is performed along the circles of latitudes and L describes the length of the parallels. Since the average vertical velocity in the stratosphere is generally considered negligible (Sun et al., 2023), no filtering is applied on the pressure-coordinate vertical velocity ω and we use $\omega' = \omega$ for the perturbation part. For the lower vertical levels, the integrands of the momentum fluxes are additionally multiplied by the factor $n = -\rho g \partial z/\partial p$ for the density ρ, gravitational acceleration g, altitude z and pressure p to account for possible deviations from hydrostatic equilibrium; see Appendix A of Procházková et al. (2025) for derivation of this term. Note that with the definition of Eqs. (1) and (2), the momentum flux is defined in the pressure coordinates with the units of $\mathrm{m\,Pa\,s^{-2}}$. For conversion into units of Pa, as is usual in the z-coordinate systems, the fluxes in the figures are multiplied by $-1/g$ with $g = 9.81\,\mathrm{ms^{-2}}$. This multiplicative factor can be derived from the fact that the drag exerted by the flux in pressure coordinates (computed as the pressure derivative of the flux) should be the same as the drag in z-coordinates (computed as the derivative with respect to the altitude).

Since Eqs. (1) and (2) contain averaging over the latitude, the data provide reasonable estimates whenever the circle of constant latitude is longer than the wavelength of the waves admitted by the filtering. For the rho20 method, this implies reliability of the estimates in the polar regions up to approximately 87°, for the rho40 method up to 88°, although more smooth estimates can be obtained further from the poles.

In the meridional direction, the dataset keeps the original resolution $0.28°$ of the full T639 ERA5 grid. Together with the high-resolution of the 36 vertical levels and daily temporal resolution, the dataset provides unusually detailed information on the zonal averages of GW momentum fluxes. In the next sections, we will validate the data and show how their properties can be utilized for atmospheric research.

2.1 Validation of the data

To validate the zonal mean vertical fluxes of zonal and meridional momentum due to GWs resolved in ERA5, we first average the fluxes over the full timespan of the data and analyze their climatological distribution in a meridional plane. As visualized in Fig. 1 for northern hemispheric winter (DJF) and summer (JJA), maximal GW momentum fluxes can be observed at the lowest levels of our analysis. In the winter hemispheres, we see strong zonal mean upward transport of westward momentum (in short, negative zonal momentum flux) reaching to the upmost vertical levels of the data. In the summer hemispheres, the negative zonal momentum flux has a smaller magnitude and is confined to the subtropical jet and its vicinity. In the equatorial region,

https://doi.org/10.5194/essd-2026-782
Preprint. Discussion started: 22 November 2026
© Author(s) 2026. CC BY 4.0 License.

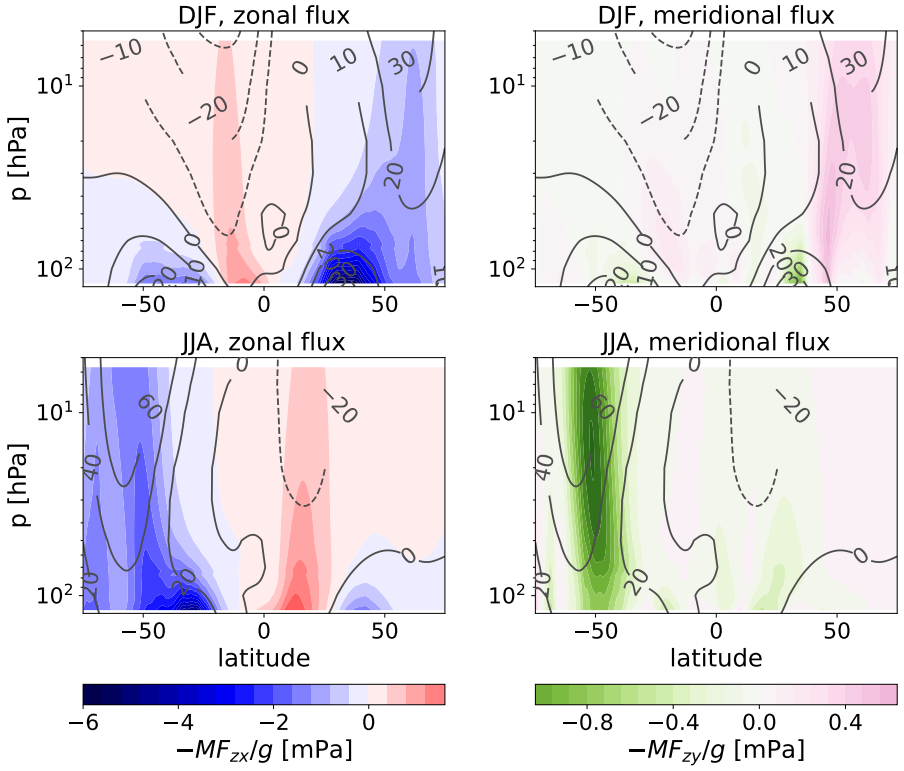

Figure 1. Zonal mean zonal (first column) and meridional (second column) flux, averaged over the 44 years for boreal winter (first row) and summer (second row). Contour lines visualize the zonal mean zonal wind. As expected, the flux amplitudes are maximal above subtropical jet stream and near the polar vortex.

Fig. 1 shows a positive vertical flux of zonal momentum broadening towards the summer hemisphere with height in the zone of negative zonal mean zonal winds. For both signs of the flux, the decrease of amplitude with height implies GW dissipation, deposition of the momentum and resulting drag with a magnitude directly proportional to the steepness of the decrease and of the same sign as the vertical flux.

The zonal mean vertical flux of meridional momentum displays the strongest positive values in the stratosphere around 50°N and negative around 50°S in the winter hemisphere, suggesting transport of poleward momentum from GWs towards the polar vortex (poleward meridional momentum flux is positive in the Northern Hemisphere and negative in the Southern Hemisphere). In general, the zonal mean momentum flux is similar to what would be expected based on previous understanding of oblique propagation of GWs towards the center of the jet (Kruse et al., 2023) and is consistent with the momentum fluxes for lower pressure levels computed by Gupta et al. (2024c, Fig. 3), showing similar momentum fluxes in their highest levels.

In the next step, we compare the ERA5 based momentum fluxes with satellite observations–the HIRDLS (High Resolution Dynamics Limb Sounder; Gille et al., 2003) based part of the GRACILE dataset (Ern et al., 2018). However, for satellite observations of temperature, as is the case for HIRLDS, only absolute pseudomomentum fluxes can be inferred using the

https://doi.org/10.5194/essd-2026-782
Preprint. Discussion started: 22 November 2026
© Author(s) 2026. CC BY 4.0 License.



method of (Ern et al., 2004),

$$pMF_{abs} = \frac{1}{2}\left(\frac{g}{N}\right)^2 \left(\frac{\hat{T}}{\overline{T}}\right)^2 . \tag{3}$$

In the equation, g is the gravity, N is the buoyancy frequency, $\overline{T}$ is the mean temperature and $\hat{T}$ is the GW temperature amplitude.

Assuming mid-frequency part of the GW spectrum, this quantity approximates the pseudomomentum fluxes, as defined by equation

$$(pMF_{zx}, pMF_{zy}) = \bar{\rho}\left(1 - \frac{f^2}{\hat{\omega}^2}\right)\left(\overline{u'w'}, \overline{v'w'}\right). \tag{4}$$

Here, $\bar{\rho}$ is the mean density, f is the Coriolis parameter, $\hat{\omega}$ is the intrinsic frequency and u', v' and w' are wave perturbations of the wind components. The absolute pseudomomentum flux from GRACILE is then related to the pseudomomentum flux as $pMF_{abs} = \sqrt{(pMF_{zx})^2 + (pMF_{zy})^2}$.

Here we compare the absolute pseudomomentum flux from Eq. (3) with the ERA5 based absolute momentum flux computed as $MF_{abs} = \sqrt{MF_{zx}^2 + MF_{zy}^2}$. Since we are comparing momentum and pseudomomentum fluxes, we cannot expect a precise match of the fields. Basically, we expect the pseudomomentum fluxes to be smaller compared to our momentum flux estimates by the variable factor $(1 - f^2/\hat{\omega}^2)$. As the GRACILE dataset contains also a climatology of horizontal and vertical wavenumbers, dispersion relation for GWs is further applied to approximate this term and obtain estimates of the momentum fluxes based on the HIRDLS data.

The absolute momentum and pseudomomentum flux is compared for the period from March 2005 to February 2008, matching the time span of the GRACILE dataset. Figure 2 shows the comparison of the averaged vertical profiles for DJF and JJA. For the HIRDLS data, the figure visualizes both the pseudomomentum flux directly obtained from the GRACILE dataset and the estimates of the corresponding momentum flux interpolated to pressure levels. However, the two profiles do not qualitatively differ, which justifies the comparison of the ERA5 momentum flux estimates with the HIRDLS pseudomomentum fluxes. At first glance, the values of the absolute momentum flux in ERA5 are smaller compared to the HIRDLS ones, although the spatial distribution of the fluxes is similar. The lower magnitude of the ERA5 momentum fluxes can be expected due to the lower horizontal resolution of ERA5. This is consistent with findings of Gupta et al. (2024c), showing that the momentum fluxes due to GWs resolved by ERA5 are significantly weaker compared to fluxes present in a 1km simulation of the IFS model, although the flux distribution is correct. The fluxes computed by the rho40 method are even lower than the fluxes visualized in Fig. 2 due to the narrower spectrum of considered wave perturbations (see Supplement).

Another difference between the datasets is the more detailed vertical and meridional structure of the ERA5 based momentum fluxes due to the high latitudinal and vertical resolution of the dataset, allowing us to observe for example two maxima in the momentum fluxes for the mid and high latitudes in the Northern Hemisphere during DJF. This double peak structure remains hidden in the HIRDLS data. For JJA in the Southern Hemisphere, these two maxima are again clearly present in ERA5. However, in this case, HIRDLS is limited by the latitudinal range of the data, which do not cover the southern-hemispheric polar region.

https://doi.org/10.5194/essd-2026-782
Preprint. Discussion started: 22 November 2026
© Author(s) 2026. CC BY 4.0 License.

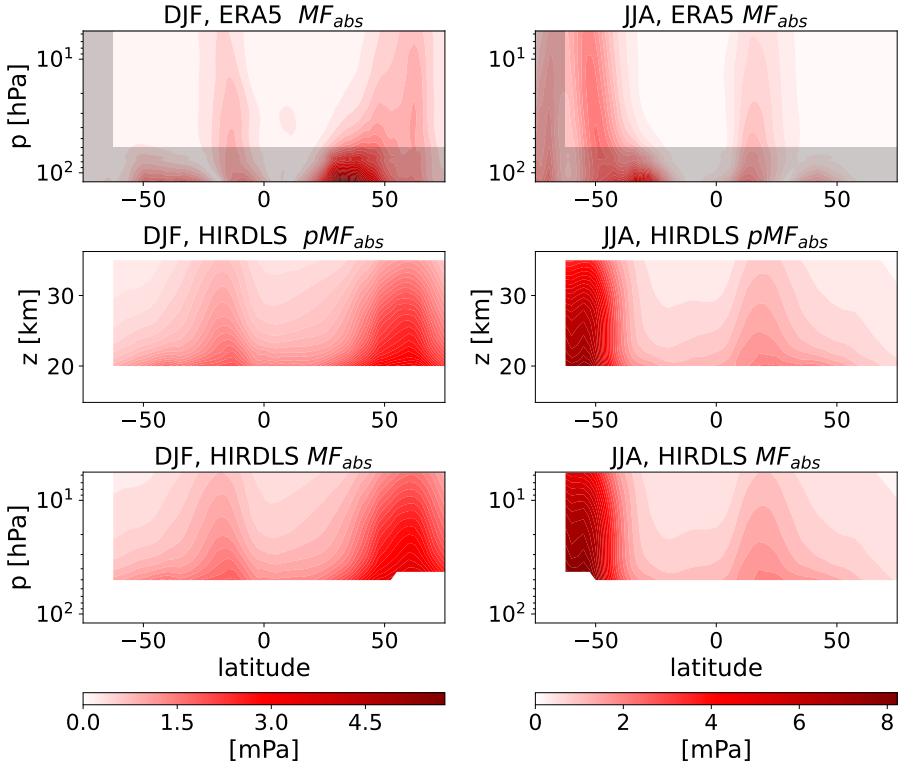

Figure 2. Absolute momentum and pseudomomentum flux for DJF and JJA between for ERA5 (first row) and HIRDLS data from the GRACILE dataset (second row). To simplify the comparison, pseudomomentum flux from HIRDLS was converted to momentum flux and interpolated on pressure levels (third row). The range of altitudes and latitudes unavailable by HIRDLS is denoted by the shaded region. The fluxes from ERA5 have similar profiles but lower magnitude compared to the HIRDLS data.

Going beyond the climatology, the temporal evolution of the fluxes for both datasets is shown for selected altitudes in Figs. 3 and 4. To be able to visualize the differences between the structure with the different magnitudes, as discussed above, the ERA5 momentum fluxes in these figures are artificially multiplied by a factor of 2.

First, we focus on the time evolution of the fluxes at the altitude of 35 km (topmost level where data from both datasets are available) shown in Fig. 3. The structure of the fluxes between the datasets is very similar, with the maximum fluxes at the Southern Hemisphere in July and August at approximately 50°S. The distribution of the momentum fluxes of ERA5 in lower altitudes also closely resembles the distribution observed by the HIRDLS instrument. However, in ERA5, the periods of higher fluxes in the subtropics alternate rather between the Southern and Northern hemisphere, whereas in HIRDLS data, there are also months without any pronounced maximum. This can be related to a higher level of background noise in the GRACILE dataset and the reduction of the noise is a clear improvement of the flux estimates.

https://doi.org/10.5194/essd-2026-782
Preprint. Discussion started: 22 November 2026
© Author(s) 2026. CC BY 4.0 License.



Open Access Earth System Science Data Discussions

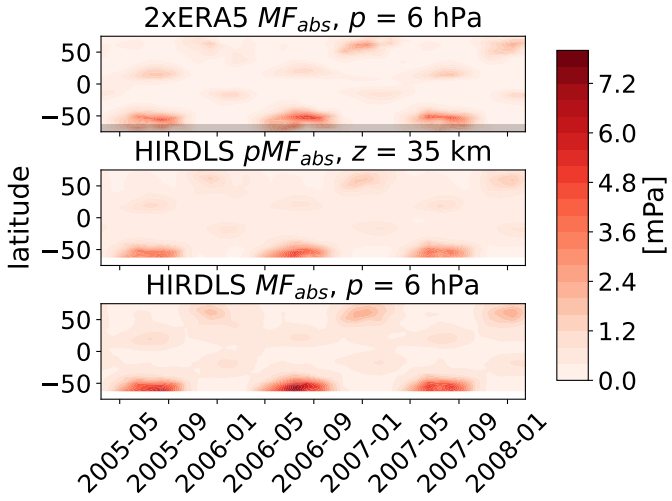

Figure 3. Absolute momentum and pseudomomentum flux for ERA5 (first subplot) and HIRDLS data from the GRACILE dataset (second subplot) for the altitude of 35 km/6 hPa. In the third subplot, the pseudomomentum flux from HIRDLS was converted to momentum flux and interpolated to pressure levels. Momentum flux from ERA5 was multiplied by 2 to simplify the comparison. The time evolution is similar for both the datasets.

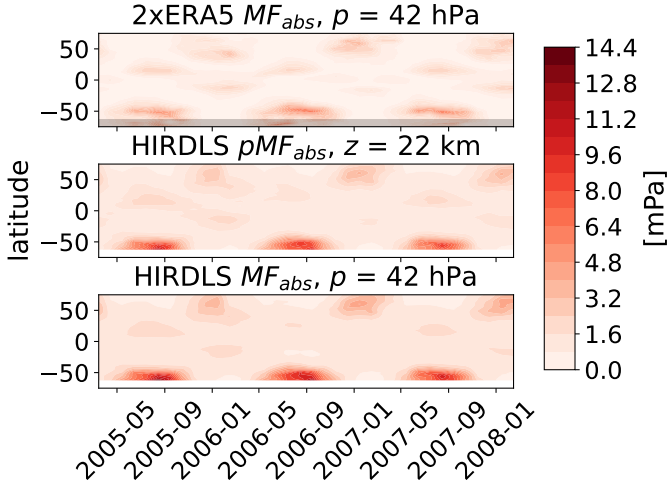

Figure 4. Same as Fig. 3 but for the altitude of 22 km/42 hPa. The datasets differ especially for lower latitudes.

The difference between background noise is also pronounced in Fig. 4 for the altitude of 20 km. For this altitude, the structure of the fluxes between the datasets however differs both in terms of the polar maxima and the structure in the lower latitudes. A possible cause for the difference is the decreasing precision of the HIRDLS data with decreasing altitude (Ern et al., 2018).

https://doi.org/10.5194/essd-2026-782
Preprint. Discussion started: 22 November 2026
© Author(s) 2026. CC BY 4.0 License.

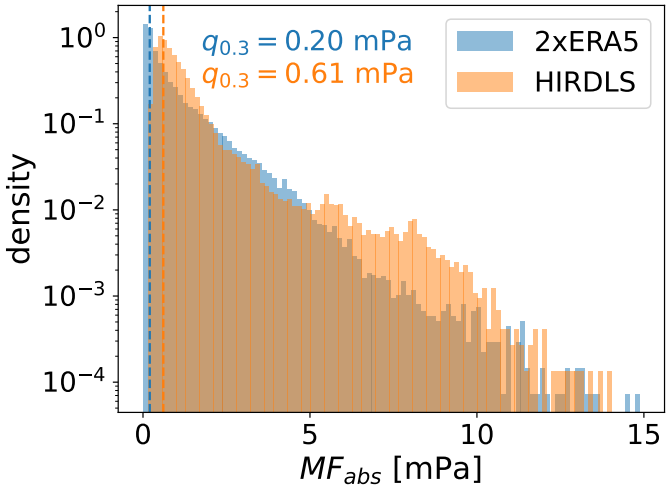

Figure 5. Distribution of the monthly mean absolute momentum flux from HIRDLS and ERA5 for the time period of the HIRDLS data interpolated to the pressure levels of ERA5 data. To simplify the comparison, ERA5 momentum fluxes are multiplied by a factor of 2. Dashed vertical lines in the plot denote 30th percentile of HIRDLS and 2xERA5 momentum fluxes. For both datasets, the occurrence frequencies are mostly decreasing with increasing momentum fluxes, with an almost uniform slope in ERA5.

The higher background level of absolute momentum flux of the HIRDLS data can also be confirmed by the statistical distribution of the momentum flux values (Fig. 5). For ERA5, the absolute momentum flux is for most timesteps and pressure levels below 0.07 mPa, while for HIRDLS data, the highest frequency of occurrence is shifted from zero to a range of fluxes between 0.4 and 0.6 mPa. This shift in the occurrence of low values is also apparent from the 30th percentiles visualised in Fig. 5, with values of 0.1 mPa for ERA5 and 0.6 mPa for HIRDLS data. In addition, there are more frequent fluxes in the range 5–10 mPa (the distribution is less steep in this range), possibly corresponding to the reduced structure of the local maxima in Figs. 3 and 4. Notably, a shift of the maximum momentum flux of ERA5 towards small values was also observed by Gupta et al. (2024c), explained by unresolved small-scale waves and the lower momentum flux produced by the waves in the reanalysis. In our case, the difference in the distribution of ERA5 and the HIRDLS observation is, however, more pronounced (see histogram of the cube root of the momentum flux in Fig. S13 in the Supplement for a straight-forward comparison with Fig. 6 of Gupta et al., 2024c)

2.2 Examples of potential application

After discussing the validity of the dataset, we will further present its unique properties by illustrating potential applications in GW related research. As the dataset contains 44 years of momentum fluxes, it can be used for a long-term study of phenomena such as the QBO. Figs. 6 and 7 show the time evolution of zonal and meridional momentum fluxes, averaged over the equatorial region, driving the QBO in zonal mean zonal winds.

https://doi.org/10.5194/essd-2026-782
Preprint. Discussion started: 22 November 2026
© Author(s) 2026. CC BY 4.0 License.

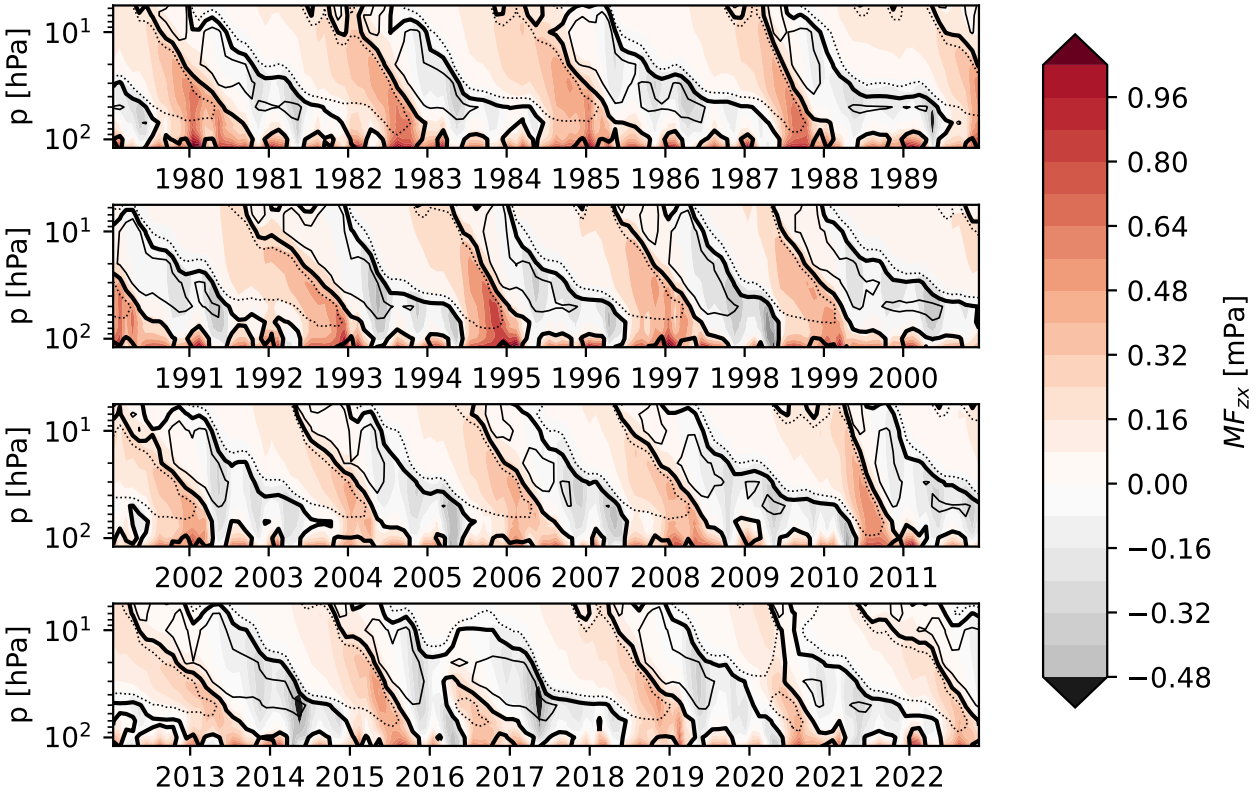

Figure 6. Time evolution of the vertical flux of zonal momentum, zonal mean averaged between 5°S and 5°N. Thick black line denotes zero zonal wind, thin solid and dotted lines denote contours $+10\,\mathrm{ms}^{-1}$ and $-10\,\mathrm{ms}^{-1}$. Regions with positive momentum flux coincide with the negative (easterly) QBO phase.

Regarding the zonal momentum fluxes in Fig. 6, the figure clearly illustrates the wave filtering mechanism by the wind field Pahlavan et al. (2023). As the momentum flux of waves propagating in the same direction as the mean flow is being reduced, we can observe a negative vertical flux of zonal momentum (easterly flux) during the westerly phase and a positive upward flux of zonal momentum (westerly flux) in the easterly QBO phase. Both negative and positive fluxes get maximal amplitudes at the levels of wind reversal. The positive momentum fluxes are generally present during the entire westerly QBO phase, whereas negative fluxes during the easterly QBO phase are exerted mostly during two to three separated events.

The meridional momentum fluxes shown in Fig. 7 exhibit a yearly cycle with positive fluxes (upward fluxes of northward momentum) during the first half of the year and negative fluxes (upward fluxes of southward momentum) during the second half of the year, accounting for the yearly changes in the mean meridional circulation within the same vertical and latitudinal range. The same fluxes as in Fig. 7 but with the meridional wind contours are displayed in Fig. S12 in the Supplement. Both negative and positive meridional momentum fluxes are stronger within the westerly QBO phase.

https://doi.org/10.5194/essd-2026-782
Preprint. Discussion started: 22 November 2026
© Author(s) 2026. CC BY 4.0 License.

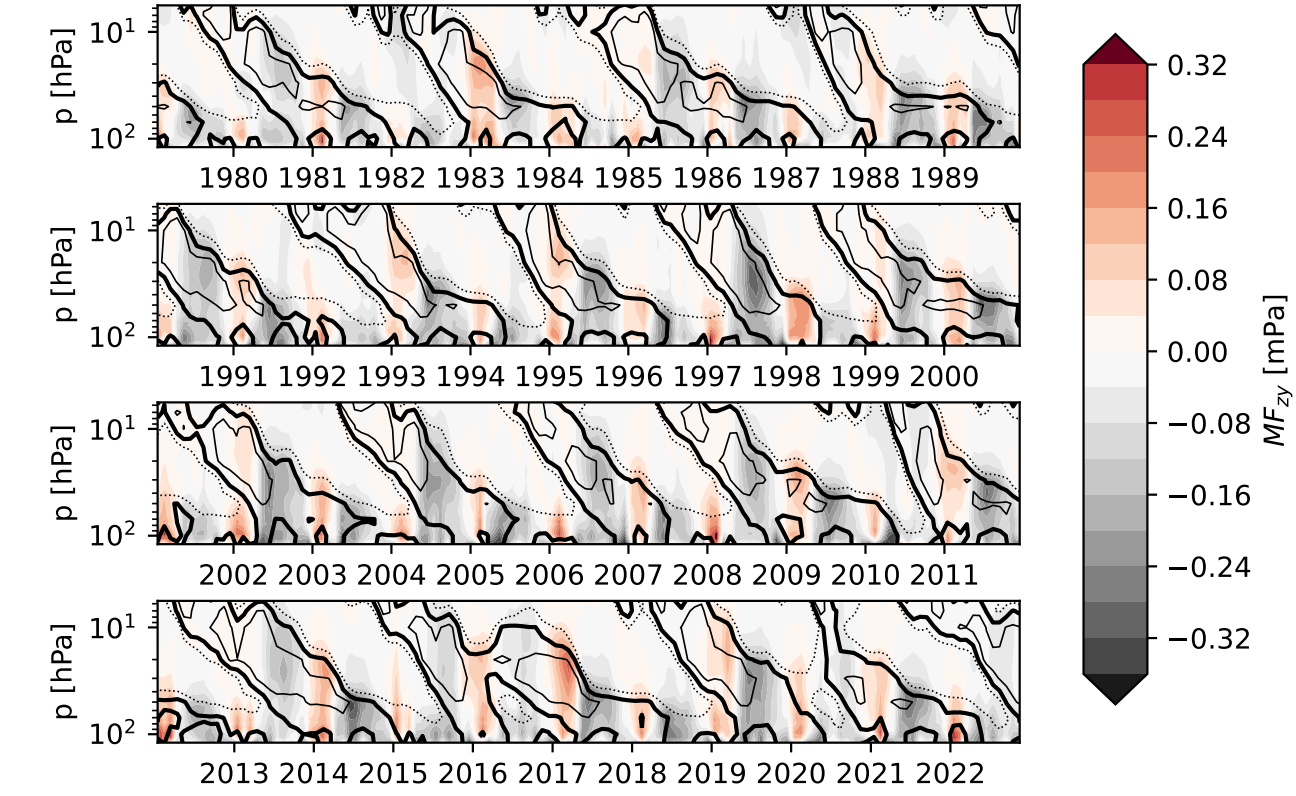

Figure 7. Time evolution of the vertical flux of meridional momentum, zonal mean averaged between 5°S and 5°N. Thick black line denotes zero zonal wind, thin solid and dotted lines denote contours $+10\,\mathrm{ms}^{-1}$ and $-10\,\mathrm{ms}^{-1}$. The meridional fluxes are stronger in the positive (westerly) QBO phase.

Since the methodology selects wave perturbation based on the horizontal wavelength, other types of waves than just GWs can be present in the equatorial region. In particular, with the upper limit on wavelength 2000 km of the rho20 method, mixed Rossby-gravity waves, together with inertia-gravity waves (GWs with longer horizontal wavelengths for which the Coriolis effect becomes more important), may also be partially captured in the data. To identify the effect of these longer waves, the difference between the zonal momentum flux estimates with rho20 and rho40 methods is shown in Fig. 8, visualizing the momentum fluxes caused by waves with horizontal wavelengths 1000 – 2000 km. Apart from a small negative contribution to the fluxes during the positive QBO phase, these longer waves contribute mostly to the positive fluxes in the negative QBO phase, supplementing around a third of the net momentum flux caused by waves with wavelengths below 2000 km (Fig. 6). This is complementary to the results of Pahlavan et al. (2023), who have shown that low-frequency waves with frequencies below 0.5 $\mathrm{rad\,d}^{-1}$ contribute only to positive fluxes. Regarding the meridional flux of vertical momentum, waves above 1000 km form about half of the fluxes from all waves below 2000 km (Fig. S8 in the Supplement), with the same structure as in Fig. 7.

https://doi.org/10.5194/essd-2026-782
Preprint. Discussion started: 22 November 2026
© Author(s) 2026. CC BY 4.0 License.

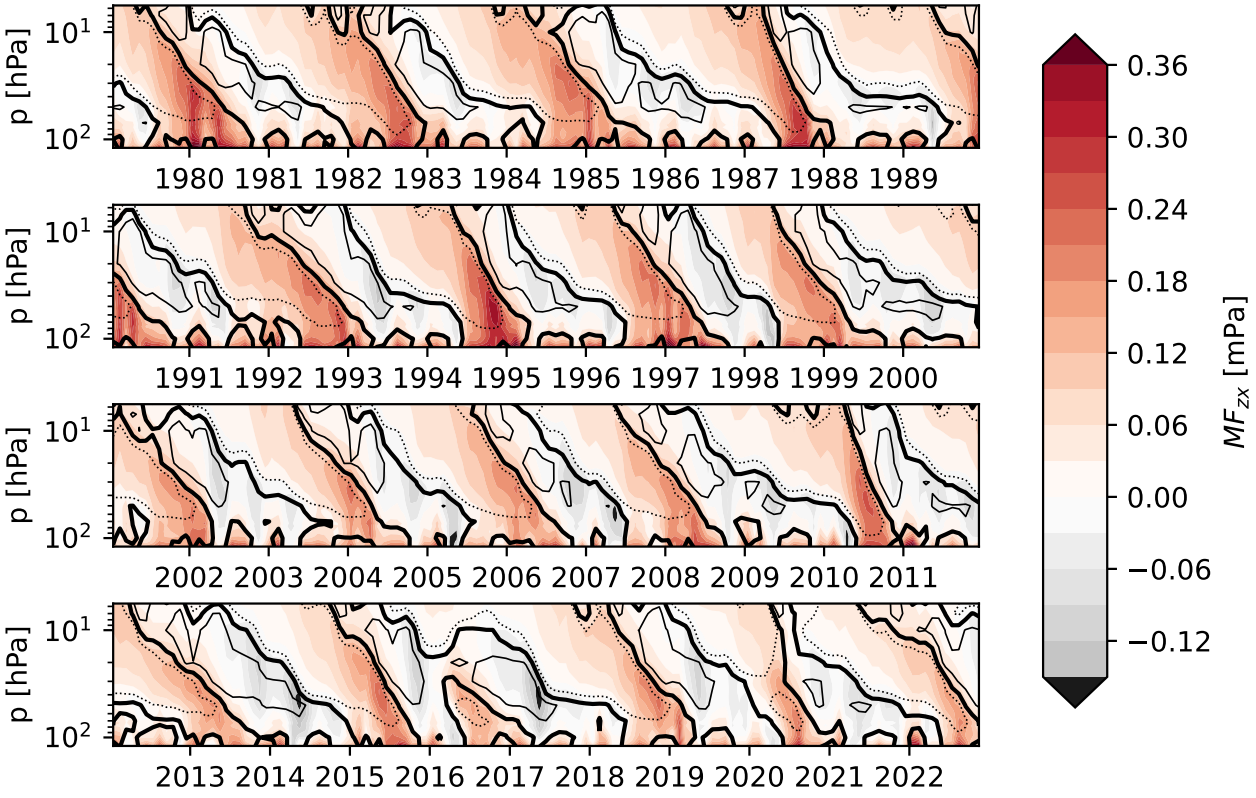

Figure 8. Time evolution of the vertical flux of zonal momentum, zonal mean averaged between 5°S and 5°N, for the waves with wavelengths between 1000 and 2000 km. Thick black line denotes zero zonal wind, thin solid and dotted lines denote contours $+10\,\mathrm{ms}^{-1}$ and $-10\,\mathrm{ms}^{-1}$. The figure shows dominance of the positive momentum flux during the easterly QBO phase and weak negative flux in the westerly phase.

The extended period covered by the dataset allows us to follow the changes in the fluxes underlying the changes in the QBO over many cycles. Additionally, we can also focus on the fluxes during particular periods in detail thanks to the high temporal resolution of our dataset. In Fig. 9, the time evolution of the zonal mean zonal and meridional momentum fluxes is plotted based on the daily averages for the QBO disruption event in 2016. From this we can observe the highly intermittent character of the waves, with strong day-to-day variations of the strength of the momentum fluxes, shown especially in the negative values of vertical flux of zonal momentum. The figure also shows a fast transition from strong negative fluxes to positive values between April and June 2016, depositing negative momentum to the flow and contributing to the disruption.

As shown by previous studies, QBO phases are also related to variability in the extratropical regions (e.g., Kawatani et al., 2019; Li et al., 2020). This is also visible in the composites of the momentum fluxes in the westward and eastward QBO phases, as shown in Fig. 10. Apart from the decrease in the flux of zonal momentum in the equatorial region by 0.6 mPa during the westward phase, changes in the momentum fluxes relatable to the Hoton-Tan effect (Holton and Tan, 1980) in the winter hemisphere are present at around 50°latitude. To be noted is that the precise structure of the plot in the equatorial region

https://doi.org/10.5194/essd-2026-782
Preprint. Discussion started: 22 November 2026
© Author(s) 2026. CC BY 4.0 License.

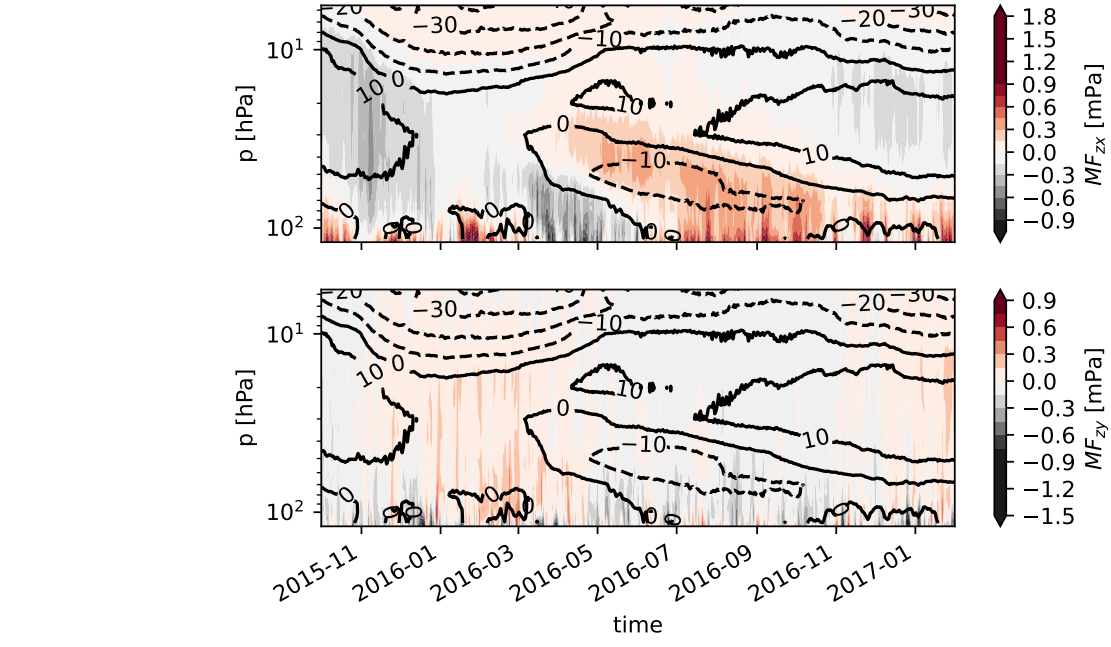

Figure 9. Momentum flux around the QBO disruption, average between 5°S and 5 °N. Contours visualize average zonal mean zonal wind for the same latitudes.

depends on the definition of the QBO phases - the figure presented here is based on the monthly mean zonal wind at 50 hPa, as available in Kerzenmacher and Braesicke (2026).

Finally, the momentum flux data can be utilized for SSW research. We will illustrate this by the evolution of the fluxes around the major SSW in 2010. Within the event, the wind decelerated rapidly at the end of January 2010, when the polar vortex shifted towards Europe, and the wind at 60°N stayed weak until the end of March (Straub et al., 2012). In Fig. 11, we show the zonal mean zonal and meridional flux before and after the onset of the SSW. In the figure, the onset of the SSW on 24 January characterized as the wind reversal above 10 hPa and north of 60 °N is visualized by the yellow line. After this date, a strong increase in the vertical flux of zonal momentum can be observed from values around -2 mPa to values close to zero. Additionally, the vertical flux of the meridional momentum decreased to zero from values around 0.6 mPa, implying a decrease in the transport of the northward momentum due to GWS after the onset of SSW. This decrease in GW momentum flux magnitude during SSW is consistent with previous studies (Ern et al., 2016; Liu, 2017) and demonstrates the utility of the presented dataset.

https://doi.org/10.5194/essd-2026-782
Preprint. Discussion started: 22 November 2026
© Author(s) 2026. CC BY 4.0 License.



Open Access Earth System Science Data Discussions

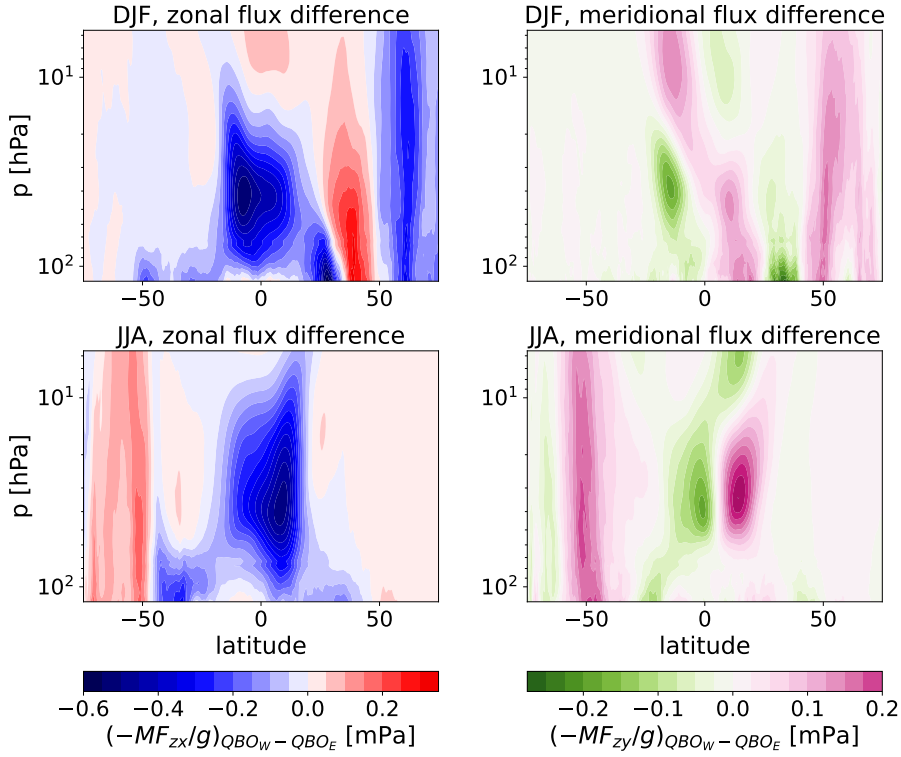

Figure 10. Composites of momentum fluxes within westward and eastward QBO phases for DJF (first row) and JJA (second row), computed from the period 1979 – 2015 to avoid years with QBO disruptions. The figure shows a strong difference in the equatorial region and near the winter pole.

3 Code and data availability

The presented dataset of time series of the zonal and meridional momentum fluxes can be accessed in the Zenodo repository at https://doi.org/10.5281/zenodo.22899283 (Procházková and Šácha, 2026). During the public peer review, the dataset will remain restricted in Zenodo. Authenticated users may request access through the Zenodo record; access requests will be approved by the data owner. Upon acceptance of the manuscript, the restrictions will be removed and the data files will be made publicly available.

In the paper, zonal wind averages data from the study Serva et al. (2024) available at https://doi.org/10.5281/zenodo.7081436 (Serva, 2022) were used. For the description of the QBO phases, data from the repository https://doi.org/10.5281/zenodo.21758978 (Kerzenmacher and Braesicke, 2026) were taken. HIRDLS pseudomomentum fluxes were taken from the GRACILE dataset at https://doi.org/10.1594/PANGAEA.879658 (Ern et al., 2018).

The codes used to produce the dataset from the publicly available ERA5 data (Hersbach et al., 2020) are available within the package of Procházková et al. (2025) (https://doi.org/10.5281/zenodo.17020639).

https://doi.org/10.5194/essd-2026-782
Preprint. Discussion started: 22 November 2026
© Author(s) 2026. CC BY 4.0 License.



Open Access Earth System Science Data Discussions

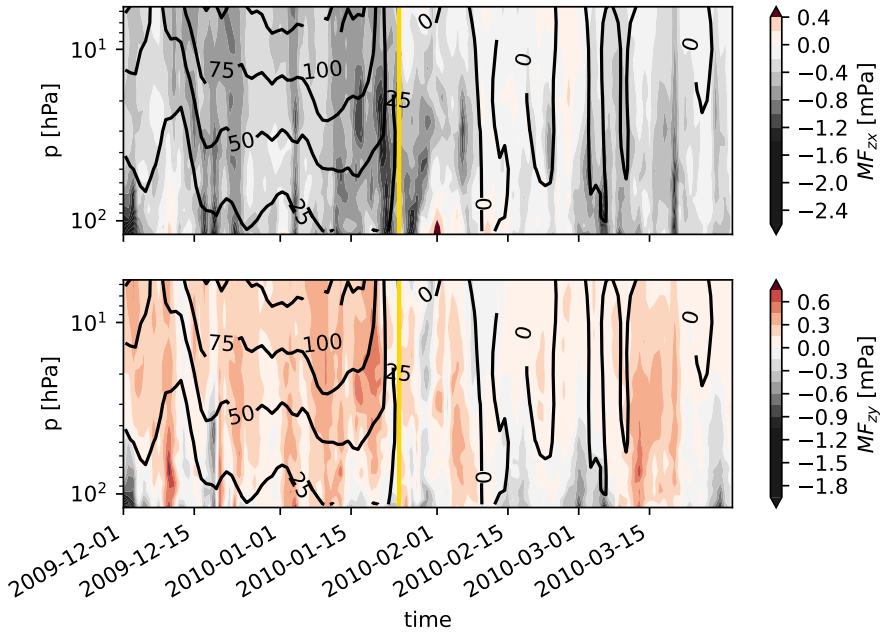

Figure 11. Momentum flux around SSW on January 24, 2010 at 60°N. Contours visualise zonal mean zonal wind at 60°N. The magnitude of the flux decreases after the onset of the SSW denoted by the yellow vertical line.

4 Conclusions

The ERA5 reanalysis is a valuable resource for studies of GWs in the stratosphere (e.g., Pahlavan et al., 2023; Gupta et al., 2021, 2024b; Cullens and Thurairajah, 2021). Here, we used the reanalysis data to create a unique dataset of resolved zonally averaged vertical fluxes of zonal and meridional momentum with unprecedented temporal, latitudinal and vertical resolution and time span of 44 years.

From comparison with the GRACILE data, we have shown that the magnitude of the momentum fluxes in ERA5 is underestimated. This is most likely due to the fact that ERA5 does not resolve the shortest GWs. This underestimation of the GW amplitudes was also observed in the previous literature. However, the distribution of waves has also previously been shown to match the distribution of waves in high-resolution simulations or satellite observation (Lear et al., 2024; Gupta et al., 2024c). Similarly, in the presented dataset, both the spatial structure of the average zonal mean fluxes and the time evolution were comparable to the GRACILE data. Apart from the longer time span and higher reliability in the lower altitudes, the advantage of the ERA5 flux estimates is lower noise, as high noise levels in observations complicate the analysis of GWs in satellite data (Okui et al., 2025).

In the last part of the paper, we have shown the utility of the data for the research of dynamical processes shaping the phenomena such as QBO or SSWs. The momentum fluxes can be used for analyzing the GW activity during individual QBO phases or for studying the dynamics for specific events of interest thanks to the high temporal resolution of the dataset. Since

https://doi.org/10.5194/essd-2026-782
Preprint. Discussion started: 22 November 2026
© Author(s) 2026. CC BY 4.0 License.



the dataset contains separate momentum flux estimates for the resolved GW spectrum with wavelengths under 1000 and 2000 km, the contribution of longer wave modes such as the inertia-gravity waves can be disentangled for all time instances and across the spatial extent of the data. In summary, we recommend the presented dataset as a complementing resource for all types of GW studies, allowing for research of long-term evolution and changes, as well as detailed analyzes of dynamics for events of interest. It also enables robust evaluation of the GW field in high-resolution models and can be used to inform GW parameterization development.

Author contributions. ZP: preparation of the dataset, analysis of the data, methodology. PŠ: conceptualization. Both authors contributed to writing.

Competing interests. The authors declare that they have no conflict of interest.

Acknowledgements. We thank Dr. Manfred Ern for providing pressure and buoyancy frequency from HIRDLS data, which simplified the comparison of the datasets. This work was supported by the GAČR JUNIOR STAR project "Unravelling climate impacts of atmospheric internal gravity waves" under 23-04921M, and made possible by using the resources of the Deutsches Klimarechenzentrum (DKRZ) granted by its Scientific Steering Committee (WLA) under project ID bm1233. Petr Šácha was also partly supported by the Charles University Research Centre program no. UNCE/24/SCI/005 and acknowledges the discussions within the International Space Science Institute (ISSI) Bern International Team project 'Impacts and Monitoring of Climate Change on the Middle and Upper Atmosphere' (#25-631).

https://doi.org/10.5194/essd-2026-782
Preprint. Discussion started: 22 November 2026
© Author(s) 2026. CC BY 4.0 License.



References

Abdalla, S.: Effective spectral resolution of ECMWF atmospheric forecast models, ECMWF Newsletter, 137, 19, https://doi.org/10.21957/rue4o7ac, 2013.

Alexander, M., Gille, J., Cavanaugh, C., Coffey, M., Craig, C., Eden, T., Francis, G., Halvorson, C., Hannigan, J., Khosravi, R., et al.: Global estimates of gravity wave momentum flux from High Resolution Dynamics Limb Sounder observations, Journal of Geophysical Research: Atmospheres, 113, https://doi.org/10.1029/2007JD008807, 2008.

Baldwin, M. P., Gray, L. J., Dunkerton, T., Hamilton, K., Haynes, P., Randel, W., Holton, J. R., Alexander, M. J., Hirota, I., Horinouchi, T., et al.: The quasi-biennial oscillation, Reviews of Geophysics, 39, 179–229, https://doi.org/10.1029/1999RG000073, 2001.

Baldwin, M. P., Ayarzagüena, B., Birner, T., Butchart, N., Butler, A. H., Charlton-Perez, A. J., Domeisen, D. I., Garfinkel, C. I., Garny, H., Gerber, E. P., et al.: Sudden stratospheric warmings, Reviews of Geophysics, 59, e2020RG000 708, https://doi.org/10.1029/2020RG000708, 2021.

Cullens, C. Y. and Thurairajah, B.: Gravity wave variations and contributions to stratospheric sudden warming using long-term ERA5 model output, Journal of Atmospheric and Solar-Terrestrial Physics, 219, 105 632, https://doi.org/10.1016/j.jastp.2021.105632, 2021.

Ern, M., Preusse, P., Alexander, M. J., and Warner, C. D.: Absolute values of gravity wave momentum flux derived from satellite data, Journal of Geophysical Research: Atmospheres, 109, https://doi.org/10.1029/2004JD004752, 2004.

Ern, M., Trinh, Q. T., Kaufmann, M., Krisch, I., Preusse, P., Ungermann, J., Zhu, Y., Gille, J. C., Mlynczak, M. G., Russell III, J. M., et al.: Satellite observations of middle atmosphere gravity wave absolute momentum flux and of its vertical gradient during recent stratospheric warmings, Atmospheric Chemistry and Physics, 16, 9983–10 019, https://doi.org/10.5194/acp-16-9983-2016, 2016.

Ern, M., Trinh, Q. T., Preusse, P., Gille, J. C., Mlynczak, M. G., Russell III, J. M., and Riese, M.: GRACILE: A comprehensive climatology of atmospheric gravity wave parameters based on satellite limb soundings, Earth System Science Data, 10, 857–892, https://doi.org/10.5194/essd-10-857-2018, 2018.

Gille, J. C., Barnett, J. J., Whitney, J. G., Dials, M. A., Woodard, D., Rudolf, W. P., Lambert, A., and Mankin, W.: The High-Resolution Dynamics Limb Sounder (HIRDLS) experiment on AURA, in: Infrared Spaceborne Remote Sensing XI, vol. 5152, pp. 162–171, SPIE, https://doi.org/doi.org/10.1117/12.507657, 2003.

Gisinger, S., Polichtchouk, I., Dörnbrack, A., Reichert, R., Kaifler, B., Kaifler, N., Rapp, M., and Sandu, I.: Gravity-Wave-Driven Seasonal Variability of Temperature Differences Between ECMWF IFS and Rayleigh Lidar Measurements in the Lee of the Southern Andes, Journal of Geophysical Research: Atmospheres, 127, e2021JD036 270, https://doi.org/10.1029/2021JD036270, 2022.

Green, B., Sheshadri, A., Alexander, M. J., Bramberger, M., and Lott, F.: Gravity wave momentum fluxes estimated from Project Loon balloon data, Journal of Geophysical Research: Atmospheres, 129, e2023JD039 927, https://doi.org/10.1029/2023JD039927, 2024.

Gupta, A., Birner, T., Dörnbrack, A., and Polichtchouk, I.: Importance of gravity wave forcing for springtime southern polar vortex breakdown as revealed by ERA5, Geophysical Research Letters, 48, e2021GL092 762, https://doi.org/10.1029/2021GL092762, 2021.

Gupta, A., Reichert, R., Dörnbrack, A., Garny, H., Eichinger, R., Polichtchouk, I., Kaifler, B., and Birner, T.: Estimates of Southern hemispheric gravity wave momentum fluxes across observations, reanalyses, and kilometer-scale numerical weather prediction model, Journal of the Atmospheric Sciences, 81, 583–604, https://doi.org/10.1175/JAS-D-23-0095.1, 2024a.

Gupta, A., Sheshadri, A., Alexander, M. J., and Birner, T.: Insights on lateral gravity wave propagation in the extratropical stratosphere from 44 years of ERA5 data, Geophysical Research Letters, 51, e2024GL108 541, https://doi.org/10.1029/2024GL108541, 2024b.

https://doi.org/10.5194/essd-2026-782
Preprint. Discussion started: 22 November 2026
© Author(s) 2026. CC BY 4.0 License.



Gupta, A., Sheshadri, A., and Anantharaj, V.: Gravity wave momentum fluxes from 1 km global ECMWF integrated forecast system, Scientific Data, 11, 903, https://doi.org/10.1038/s41597-024-03699-x, 2024c.

Hersbach, H., Bell, B., Berrisford, P., Hirahara, S., Horányi, A., Muñoz-Sabater, J., Nicolas, J., Peubey, C., Radu, R., Schepers, D., et al.: The ERA5 global reanalysis, Quarterly Journal of the Royal Meteorological Society, 146, 1999–2049, https://doi.org/10.1002/qj.3803, 2020.

Hertzog, A., Alexander, M. J., and Plougonven, R.: On the intermittency of gravity wave momentum flux in the stratosphere, Journal of the Atmospheric Sciences, 69, 3433–3448, https://doi.org/10.1175/JAS-D-12-09.1, 2012.

Holton, J. R. and Tan, H.-C.: The Influence of the Equatorial Quasi-Biennial Oscillation on the Global Circulation at 50 mb, Journal of Atmospheric Sciences, 37, 2200 – 2208, https://doi.org/10.1175/1520-0469(1980)037<2200:TIOTEQ>2.0.CO;2, 1980.

Kawatani, Y., Hamilton, K., Sato, K., Dunkerton, T. J., Watanabe, S., and Kikuchi, K.: ENSO modulation of the QBO: Results from MIROC models with and without nonorographic gravity wave parameterization, Journal of the Atmospheric Sciences, 76, 3893–3917, https://doi.org/10.1175/JAS-D-19-0163.1, 2019.

Kerzenmacher, T. and Braesicke, P.: QBO: monthly zonal stratospheric winds from tropical radiosonde data (mainly Singapore) [Dataset, https://doi.org/10.5281/zenodo.21758978, 2026.

Kim, Y.-H.: Explaining the period fluctuation of the quasi-biennial oscillation, Atmospheric Chemistry and Physics, 25, 5647–5664, https://doi.org/10.5194/acp-25-5647-2025, 2025.

Klaver, R., Haarsma, R., Vidale, P. L., and Hazeleger, W.: Effective resolution in high resolution global atmospheric models for climate studies, Atmospheric Science Letters, 21, e952, https://doi.org/10.1002/asl.952, 2020.

Kruse, C. G., Richter, J. H., Alexander, M. J., Bacmeister, J. T., Heale, C., and Wei, J.: Gravity Wave Drag Parameterizations for Earth's Atmosphere, chap. 9, pp. 229–256, American Geophysical Union (AGU), ISBN 9781119529019, https://doi.org/10.1002/9781119529019.ch9, 2023.

Lear, E. J., Wright, C. J., Hindley, N. P., Polichtchouk, I., and Hoffmann, L.: Comparing gravity waves in a kilometer-scale run of the IFS to airs satellite observations and ERA5, Journal of Geophysical Research: Atmospheres, 129, e2023JD040 097, https://doi.org/10.1029/2023JD040097, 2024.

Li, Z., Chu, X., Harvey, V. L., Jandreau, J., Lu, X., Yu, Z., Zhao, J., and Fong, W.: First lidar observations of quasi-biennial oscillation-induced interannual variations of gravity wave potential energy density at McMurdo via a modulation of the Antarctic polar vortex, Journal of Geophysical Research: Atmospheres, 125, e2020JD032 866, https://doi.org/10.1029/2020JD032866, 2020.

Lim, E.-P., Hendon, H. H., Boschat, G., Hudson, D., Thompson, D. W., Dowdy, A. J., and Arblaster, J. M.: Australian hot and dry extremes induced by weakenings of the stratospheric polar vortex, Nature Geoscience, 12, 896–901, https://doi.org/10.1038/s41561-019-0456-x, 2019.

Limpasuvan, V., Richter, J. H., Orsolini, Y. J., Stordal, F., and Kvissel, O.-K.: The roles of planetary and gravity waves during a major stratospheric sudden warming as characterized in WACCM, Journal of Atmospheric and Solar-Terrestrial Physics, 78, 84–98, https://doi.org/10.1016/j.jastp.2011.03.004, 2012.

Liu, H.-L.: Gravity wave variation from the troposphere to the lower thermosphere during a stratospheric sudden warming event: A case study, SOLA, 13, 24–30, https://doi.org/10.2151/sola.13A-005, 2017.

Okui, H., Wright, C. J., Berthelemy, P. G., Hindley, N. P., Hoffmann, L., and Barnes, A. P.: A convolutional neural network for the detection of gravity waves in satellite observations and numerical simulations, Geophysical Research Letters, 52, e2025GL115 683, https://doi.org/10.1029/2025GL115683, 2025.

https://doi.org/10.5194/essd-2026-782
Preprint. Discussion started: 22 November 2026
© Author(s) 2026. CC BY 4.0 License.



Pahlavan, H. A., Wallace, J. M., and Fu, Q.: Characteristics of tropical convective gravity waves resolved by ERA5 reanalysis, Journal of the Atmospheric Sciences, 80, 777–795, https://doi.org/10.1175/JAS-D-22-0057.1, 2023.

Procházková, Z., Zajíček, R., and Šácha, P.: Climatology, long-term variability and trend of resolved gravity wave drag in the stratosphere revealed by ERA5, Weather and Climate Dynamics, 6, 927–947, https://doi.org/10.5194/wcd-6-927-2025, 2025.

Procházková, Z., Zajíček, R., and Šácha, P.: prochazz/era5gws: Gravity wave fluxes and drag [Comuputer software], https://doi.org/10.5281/zenodo.17020639, Zenodo, 2025.

Procházková, Z. and Šácha, P.: Daily values of resolved zonal-mean momentum fluxes based on ERA5 [Dataset], https://doi.org/10.5281/zenodo.22899283, Zenodo, 2026.

Richter, J. H., Anstey, J. A., Butchart, N., Kawatani, Y., Meehl, G. A., Osprey, S., and Simpson, I. R.: Progress in simulating the quasi-biennial oscillation in CMIP models, Journal of Geophysical Research: Atmospheres, 125, e2019JD032 362, https://doi.org/10.1029/2019JD032362, 2020.

Serva, F.: Transformed Eulerian mean data from the ERA5 reanalysis (daily means) (Version 0.1.1) [Dataset], https://doi.org/10.5281/zenodo.7081436, Zenodo, 2022.

Serva, F., Christiansen, B., Davini, P., Von Hardenberg, J., Van Den Oord, G., Reerink, T., Wyser, K., and Yang, S.: Changes in stratospheric dynamics simulated by the EC-Earth model from CMIP5 to CMIP6, Journal of Advances in Modeling Earth Systems, 16, e2023MS003 756, https://doi.org/10.1029/2023MS003756, 2024.

Simmons, A., Soci, C., Nicolas, J., Bell, B., Berrisford, P., Dragani, R., Flemming, J., Haimberger, L., Healy, S., Hersbach, H., et al.: ERA5.1: Rerun of the Fifth generation of ECMWF atmospheric reanalyses of the global climate (2000-2006 only), Copernicus Climate Change Service (C3S) Data Store (CDS), https://doi.org/10.24381/cds.143582cf, data distribution by the German Climate Computing Center (DKRZ), 2020.

Straub, C., Tschanz, B., Hocke, K., Kämpfer, N., and Smith, A. K.: Transport of mesospheric H 2 O during and after the stratospheric sudden warming of January 2010: observation and simulation, Atmospheric chemistry and physics, 12, 5413–5427, https://doi.org/10.5194/acp-12-5413-2012, 2012.

Sun, Y. Q., Hassanzadeh, P., Alexander, M. J., and Kruse, C. G.: Quantifying 3D gravity wave drag in a library of tropical convection-permitting simulations for data-driven parameterizations, Journal of Advances in Modeling Earth Systems, 15, e2022MS003 585, https://doi.org/10.1029/2022MS003585, 2023.

Wei, J., Zhang, F., Richter, J. H., Alexander, M. J., and Sun, Y. Q.: Global distributions of tropospheric and stratospheric gravity wave momentum fluxes resolved by the 9-km ECMWF experiments, Journal of the Atmospheric Sciences, 79, 2621–2644, https://doi.org/10.1175/JAS-D-21-0173.1, 2022.